Environ Fluid Mech (2007) 7:143–158
DOI 10.1007/s10652-007-9020-0

ORIGINAL ARTICLE

Energy dissipation estimates in oscillating grid setup: LDV and PIV measurements

Amer Al-Homoud · Miki Hondzo

Received: 18 April 2006/Accepted: 31 January 2007 / Published online: 6 March 2007

Abstract The dissipation of turbulent kinetic energy has been increasingly used as a scaling parameter to integrate microbiological accrual and metabolic rates with fluid-flow motion in natural and engineered aquatic ecosystems. The estimation of turbulent kinetic energy under field conditions and the generation of energy dissipation rates under controlled laboratory conditions with microbiological organisms are necessities required to integrate environmental/ecological laboratory protocols with a moving fluid in the environment. Turbulent fluid-flow conditions were generated in an oscillating grid setup, and turbulence variables were quantified using laser-Doppler velocimetry (LDV) and particle image velocimetry (PIV) measuring techniques. The rate of dissipation of the turbulent kinetic energy in the setup ranged from 10^{-9} to 10^{-4} m^2/s^3 and was similar to the levels of energy dissipation commonly reported in engineered and natural aquatic ecosystems. Time-averaged velocities were close to zero with the root-mean-square velocity ratios about 1, indicating nearly isotropic fluid-flow conditions in the setup. The velocity spectra, obtained by stationary LDV measurements for the vertical and horizontal velocity components across the setup revealed the existence of inertial subrange with the frequency power scaling law of "$\omega^{-5/3}$." The estimated Eulerian frequency spectrum followed the theoretical functional relation and confirmed the applicability of inertial dissipation method for the estimation of turbulent kinetic energy dissipation rates. PIV was used for a direct estimation of dissipation by evaluating spatially distributed velocity gradients. The direct dissipation estimate in conjunction with the estimated Eulerian frequency spectrum provided evaluation of a "universal" constant, α, commonly used for the estimation of an energy dissipation rate over the inertial subrange of the Eulerian spectrum. The results demonstrated a range of values, rather than a universal constant,

A. Al-Homoud (✉) · M. Hondzo
St. Anthony Falls Laboratory, Department of Civil Engineering, The University of Minnesota, Mississippi River at Third Avenue SE, MN 55414, Minneapolis, USA
e-mail: alho0011@umn.edu

M. Hondzo
e-mail: mhondzo@umn.edu

of α with a lognormal probability distribution for vertical and horizontal velocity components. In order to encompass a 0.955 probability range under the lognormal distribution ($\frac{\bar{\alpha}}{\sigma^2} > \alpha > \bar{\alpha}\sigma^2$) the universal constant, α, should be in the range $2.91 \geq \alpha_u \geq 0.43$ and $4.44 \geq \alpha_w \geq 0.42$ for horizontal and vertical velocity components, respectively.

Keywords Energy dissipation · Turbulence · Oscillating grid · Scaling · Microorganisms

1 Introduction

The interaction between fluid motion and microscopic aquatic organisms has received appreciable and well deserved attention over the past 10 years. New research areas, including ecohydraulics and environmental fluid mechanics, have emerged as accepted fields in the research community that emphasize the interaction among physical, chemical, and biological processes in natural and engineered aquatic ecosystems. What impact may fluid motion have on microorganisms, including bacteria and algae? Most of the microorganisms having sizes between 1–10 μm are significantly smaller than the length-scale of the smallest eddies, commonly scaled by the Kolmogorov length-scale, in natural and engineered aquatic ecosystems. The Kolmogorov length-scale, $\eta_K = \left(\frac{\nu^3}{\varepsilon}\right)^{1/4}$, determined by the rate of energy dissipation level (ε) and kinematic viscosity (ν), is on the order of $10^3\mu$m, and the corresponding smallest eddies are on the order of $10^4\mu$m. Therefore, microorganisms cannot feel the fluctuating velocity field beyond the Kolmogorov scale where the velocity perturbations are smeared by the kinematic viscosity of fluid. However, microorganisms do experience enhanced strain rates which are scaled by the rate of energy dissipation levels [1,2]. Furthermore, the enhanced strain rates mediate the diffusive sublayer thickness surrounding microorganisms and, therefore, control the uptake of nutrients and consequent biomass accrual [2,3].

While the in situ quantification of microorganisms is still a technological challenge, the recent advancements in fluid-flow measuring devices provide affordable tools to measure energy production and dissipation in natural and engineered aquatic systems from days to months. Energy dissipation rate has emerged as a meaningful scaling parameter to integrate large and small scale fluid motions with metabolic activities of microscopic organisms in aquatic ecosystems. Furthermore, most of the well established laboratory microbiological protocols such as biochemical oxygen demand [4] are designed for measuring bacterial metabolic responses in a stagnant fluid. Aquatic ecosystems are not stagnant. They continuously mediate fluid-flow energy production with energy dissipation through a variety of fluid-flow regimes ranging from laminar ("ordered") flows to less predictable turbulent flows. Subjecting microorganisms under laboratory conditions to the corresponding field estimates of energy dissipation levels will provide the necessary integration between the fluid motion and microbiological responses in aquatic ecosystems [5].

The use of the acoustic-Doppler velocimeter (ADV) is common for the unattended and prolonged in situ quantification of turbulence characteristics, including energy dissipation levels. The ADVs typically have sampling frequencies up to 50 Hz and are suited for the quantification of velocity spectral densities in the inertial subrange. The

rate of dissipation of turbulent kinetic energy, ε, can be estimated using the Eulerian frequency spectrum as proposed by Tennekes [6]

$$\phi(\omega) = \alpha \varepsilon^{2/3} u_{\text{rms}}^{2/3} \omega^{-(5/3)}, \tag{1}$$

where $\phi(\omega)$ is the kinetic energy per unit frequency ω, α a "universal" constant usually referred as the Kolmogorov constant (proposed by Tennekes on the order of 1), and u_{rms} is the horizontal root-mean-square velocity. The universality of Kolmogorov constant has been questioned since different researchers have reported various values for α being equal to 0.8 [1,7] or being in the range between 1.2 and 2 [3,5,6,8–17]. The main objective of our research was to evaluate constant α under small-scale turbulent fluid-flow conditions, which have been reported in engineered and natural aquatic ecosystems. Laboratory measurements were conducted in an oscillating grid setup using laser-Doppler velocimeter (LDV) and particle image velocimetry (PIV) in order to quantify the rate of dissipation of turbulent kinetic energy and corresponding α in the functional relation proposed by Eq. 1. The oscillating grid setup was selected because it generates nearly homogenous and isotropic turbulence under certain conditions of oscillating grid frequency, vertical distance away from the mesh, and the solidity of the grid [3,5,7,11]. The reported energy dissipation rates generated by the oscillating grid setup were also within the observed range of ε in aquatic ecosystems [3,5,18,19]. Our laboratory measurements revealed a statistical distribution for α values with the corresponding statistical moments that can be used in conjunction with Equation (1) for the estimation of the dissipation of turbulent kinetic energy.

2 Methodology

2.1 Inertial dissipation method (IDM)

The inertial dissipation method (IDM) is based on fitting measured fluctuation velocity spectra at a fixed point to their respective theoretical Eulerian form within the inertial subrange of the frequency spectrum as defined by Eq. 1. In this method it is assumed that local isotropic turbulent flow exists in the inertial subrange and that the energy production rate equals the dissipation rate. Two assumptions that underline the IDM method are: a) the slope of spectra as a function of the frequency in the inertial subrange is depicted by a −5/3 slope, and (b) the existence of a "universal" constant α that correlates the $\phi(\omega)$, ε, u_{rms}, and ω. While the existence of −5/3 slope has been widely documented, the lack of research in documenting α constrained the application of IDM method to the estimate of ε [3,5–9,11,12,17].

2.2 Direct method (DM)

Instantaneous spatial velocity measurements are used to estimate velocity gradients in order to obtain a direct estimate of ε as suggested by Doron et al. [15]

$$\varepsilon_D = 3\nu \left[\left(\frac{\partial u}{\partial x}\right)^2 + \left(\frac{\partial w}{\partial z}\right)^2 + \left(\frac{\partial u}{\partial z}\right)^2 + \left(\frac{\partial w}{\partial x}\right)^2 + 2\left(\frac{\partial u}{\partial z}\frac{\partial w}{\partial x}\right) + \frac{2}{3}\left(\frac{\partial u}{\partial x}\frac{\partial w}{\partial z}\right) \right], \tag{2}$$

where ε_D is the direct estimate of the rate of dissipation of turbulent kinetic energy, x is the coordinate in the horizontal direction, z is the coordinate in the vertical

direction; u is the horizontal velocity component in the x-direction, and w is the vertical velocity component in the z-direction. Velocity gradients are estimated variables with magnitudes heavily dependent upon the resolution of measurements in a turbulent flow. Pope [20] suggested the range of length-scales of characteristic eddies which are responsible for the bulk of the dissipation as $60 > \frac{l}{\eta_K} > 8$ where $l = \frac{2\pi}{k}$ is the wavelength corresponding to wavenumber k. This implies that velocity gradients in a turbulent flow should be resolved down to scales where $\frac{l}{\eta_K} \leq 8$ in order to accurately describe dissipative motions. At each sampling location, values of the time-averaged direct estimates of ε_D were generated as follows: (a) instantaneous velocity vector map was generated by PIV, (b) spatial velocity gradients were estimated by a central finite difference approximation of the vector velocity map, (c) the gradients were used in Eq. 2 to estimate the corresponding ε_D map, (d) the procedure was repeated for a time series of vector maps (typically 100 at one sampling location) and thus a time-averaged ε_D map was generated. The time-averaged ε_D were averaged at three vertical distances within the setup or over the LDV sampling control volume and thus provided averaged ε_D at the specific vertical distance.

3 Experimental setup

Experiments were conducted in an oscillating grid setup to replicate small-scale fluid-flow conditions in natural and engineered aquatic ecosystems. The setup consisted of a Plexiglas chamber with dimensions $50 \times 50 \times 47\,\text{cm}^3$, and a vertically oscillating grid made of square Plexiglas rods $1.3 \times 1.3 \times 48\,\text{cm}^3$ (Fig. 1). The rods were spaced 5 cm (M) apart. The grid was powered by a rotating motor with a speed controller. For each experiment, the grid was set to oscillate at frequencies of $f = 1, 2, 4$, or 6 Hz. The stroke length (S) was 3 cm. Selected frequencies in the experiments covered the range

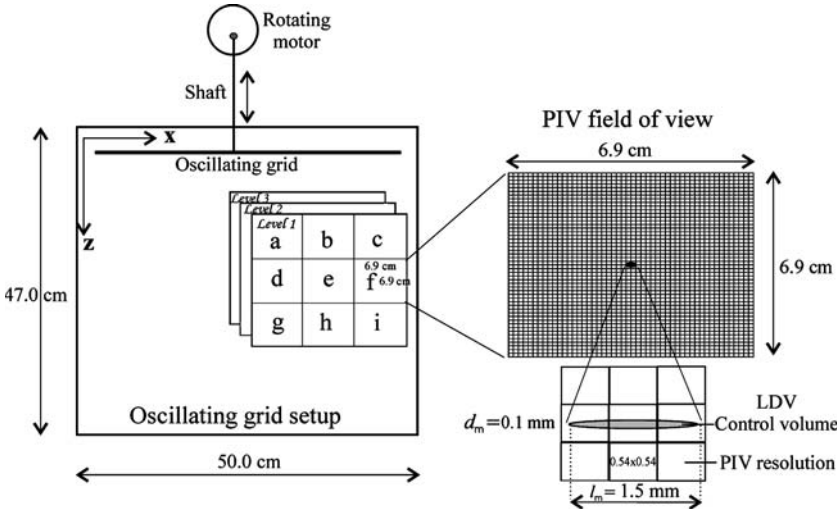

Fig. 1 Schematic of the oscillating grid setup with 27 sampling locations (9 field of views ×3 *Levels*). One particle image velocimetry (PIV) field of view ($6.9 \times 6.9\,\text{cm}^2$) and laser-Doppler velocimeter (LDV) control volume ($1.5 \times 0.1\,\text{mm}^2$) located in the center of each PIV field of view

of energy dissipation rates (ε) from 1.2×10^{-9} (at $z = 420$ mm) to 3.6×10^{-4} m^2/s^3 (at $z = 154$ mm), similar to values reported in aquatic environments [3,5,18,19]. The experimental setup provides fairly consistent reproducibility of fluid-flow conditions with the documented scaling relationships of various turbulence quantities. Furthermore, the setup contains a large volume of fluid, habitat space for microorganisms, with relatively small surface area of surrounding walls. Microorganisms including algae and bacteria tend to attach to the solid surfaces which generate additional experimental difficulties in studying microorganisms-fluid flow interactions.

4 Measurements using LDV

A LDV, manufactured by TSI (Saint Paul, MN, USA) was used to measure u and w velocities in the setup. A time series of tracer particle velocities at a point within the flow is obtained optically via light-scattering. The velocity time series consisted of 10,000 measurements at an average sampling rate of about 50 Hz. The average sampling time of 200s was significantly longer than the integral time scale of turbulence and therefore can be considered as adequate for the estimation of turbulence variables in the setup. Data were collected at four oscillating grid frequencies ($f = 1, 2, 4,$ and 6 Hz). The spatial fluid-flow velocity measurements were collected at three vertical planes (*Level* 1 to *Level* 3) evenly distributed across one quadrant of the reactor below the grid (Fig. 1). Each vertical plane consisted of nine measuring locations or field of views ("*a*" to "*i*") and thus the velocity measurements were collected at 27 sampling locations for each oscillating grid frequency. The diameter (d_m) and the volume length (l_m) of the ellipsoid sampling volume at the measurement location were approximately 0.1 and 1.5 mm, respectively (Fig. 1) (TSI specifications). The LDV sampling volume was located in the center of each field of view.

5 Measurements using PIV

A TSI PIV system consisted of a high resolution digital CCD camera, laser pulse synchronizer, pulsed laser, personal computer with TSI Insight, and data acquisition and analysis software. It was used to obtain instantaneous global two-dimensional velocity (u, w) fields in the oscillating grid setup at the exact 27 sampling locations used to obtain the temporal velocity measurements using the LDV (Fig. 1). The PIV principle involves illuminating a plane along the direction of the flow by a light sheet from a pair of Nd:Yag laser source and photographically recording the motion of tracer particles that follow the fluid-flow in the plane. The experimental setup was seeded with nominally 1 μm TiO_2. Seeding density was adjusted to ensure that there are approximately 8–10 particles pairs per interrogation window. The seed particle images were transferred into a 2048×2048 pixel CCD camera with straddle capabilities. A 60-mm focal length lens was used with an f-number of 7.2. One hundred images were taken at each measurement location with 1 Hz sampling frequency. Each pair of PIV images was interrogated using the PIV Insight software. The images were subdivided into interrogation windows of 32×32 pixels and analyzed with 50% overlap to satisfy the Nyquist criterion. The instantaneous vectors within the interrogation windows were validated and yielded 127×127 vectors per field of view with 33.78 μm/pixel that corresponds to a spatial resolution of $0.54\,\text{mm} \times 0.54\,\text{mm}^2$. The

energy dissipation rates in the oscillating grid setup ranged from 10^{-9} to 10^{-4} m^2/s^3, equivalent to the Kolmogorov length-scale from 0.2 to 5.6 mm. Therefore, a spatial resolution resolved by the PIV system was on the order of Kolmogorov length scales for the most energetic fluid-flows. A typical value for the minimum measurement error was 0.05–0.1 pixel units for a 32 × 32 pixel interrogation region as suggested by Westerweeler [21]. This implies a measurement error of 1% for a displacement that is one quarter of the interrogation window size.

6 Results and discussion

6.1 Fluid-flow velocities

Horizontal and vertical velocity measurements were obtained at all locations with LDV and PIV as described in the experimental setup. The LDV measurements provided a two-dimensional velocity time series over a sampling volume of 1.5×0.1 mm^2 located in the center of each field of view. The validated PIV interrogation windows generated 127×127 vectors per field of view with a spatial resolution of 0.54×0.54 mm per window. One hundred interrogation windows were acquired per field of view. Per field of view, 3×1 vectors (corresponding to the spatial position and dimension of LDV control volume) were used to estimate the spatial and temporal velocities measured by PIV over the LDV control volume (Fig. 1). A total of three vectors at each sampling location were augmented to obtain a time series of 3×100 data points as proposed by Bertuccioli et al. [14]. Velocity fluctuation (u' and w') were calculated from the time averaged velocities ($\bar{u}$ and $\bar{w}$) in the x and z directions, respectively. The root-mean-square turbulent velocities (u_{rms} and w_{rms}) quantify the intensity of turbulent fluctuations and their equations are defined as $u_{\text{rms}} = \overline{(u')^2})^{1/2}$ and $w_{\text{rms}} = \overline{(w')^2})^{1/2}$. An example of the velocity time series measured for 2 Hz oscillating grid frequency at $z = 222$ mm of "*Level 2*" sampling location "*e*" (Fig. 1) using the LDV and the PIV techniques is plotted in Fig. 2. Although the measurements were not simultaneously collected, and the sampling frequency with LDV was much faster than with the PIV, it is evident that the fluctuations in the time series were a similar order of magnitude and that the $\bar{u}_{\text{LDV}} = 0.0032$ m/s was comparable to the $\bar{u}_{\text{PIV}} = 0.0027$ m/s, the $u_{\text{rmsLDV}} = 0.006$ m/s was comparable to the $u_{\text{rmsPIV}} = 0.0072$ m/s; the $\bar{w}_{\text{LDV}} = 0.0033$ m/s was similar to the $\bar{w}_{\text{PIV}} = 0.0031$ m/s, and that the $w_{\text{rmsLDV}} = 0.0053$ m/s was comparable to the $w_{\text{rmsPIV}} = 0.0074$ m/s. These finding indicated that the time-averaged horizontal and vertical velocities, using both methods, were comparable with the minor presence of large-scale secondary flow cells in the setup. A comparison of the $\bar{u}$, $\bar{w}$, u_{rms}, and w_{rms} values, averaged over the entire setup, is provided in Table 1. The u_{rms} and w_{rms} ratios were in the range from 1.03 to 1.1 for the LDV measurements and 0.99–1.09 for the PIV measurements, indicating nearly isotropic rms velocities in the setup. De Silva and Fernando [22] reported w_{rms} to u_{rms} ratio in the range of 1.1 to 1.2 by LDV measurements in a similar oscillating grid setup. Webster et al. [23] reported u_{rms} to w_{rms} ratio in the range of 0.83 to 1.11 by PIV measurements.

Turbulence quantities u_{rms} and w_{rms}, both decay away with the vertical distance from the grid. The quantities at the same vertical distance in a section were averaged over the section and provided vertical variation over the experimental setup (Table 2).

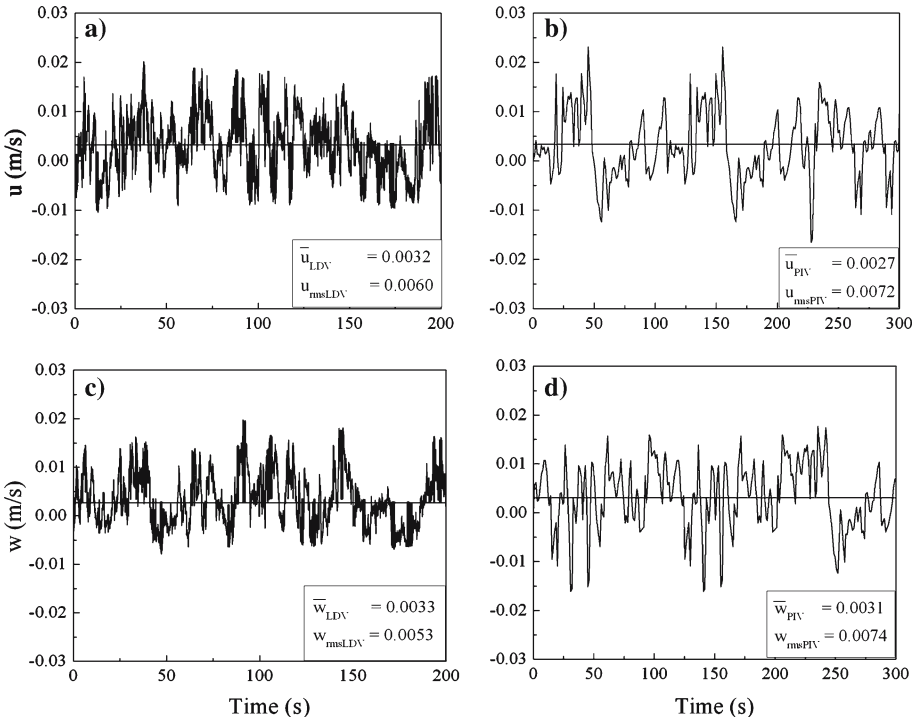

Fig. 2 Temporal horizontal (u) and vertical (w) velocity values obtained for 2 Hz oscillating frequency at $z = 222$ of *Level (2)* at location (e) using LDV with 50 Hz sampling frequency and PIV with 1 Hz sampling frequency. *a* Shows the u time record using LDV ($\bar{u}_{LDV}$) **b** the u time record using PIV ($\bar{u}_{PIV}$), **c** the w time record using LDV ($\bar{w}_{\mathrm{LDV}}$), and **d** the w time record using PIV ($\bar{w}_{\mathrm{PIV}}$)

Table 1 Comparison of fluid-flow statistics in the oscillating grid setup between LDV and PIV techniques

Grid frequency f (Hz)	LDV $\frac{\bar{w}}{\bar{u}}$	LDV $\frac{w_{\mathrm{rms}}}{u_{\mathrm{rms}}}$	PIV $\frac{\bar{w}}{\bar{u}}$	PIV $\frac{w_{\mathrm{rms}}}{u_{\mathrm{rms}}}$
1	0.84	1.09	1.32	1.08
2	1.23	1.03	1.38	1.09
4	0.97	1.08	1.13	0.98
6	0.89	1.04	1.24	1.03

PVI and LDV measurements are averaged over the oscillating grid setup

This information is particularly important for the study of chemotaxis or phototaxis where microorganisms (bacteria or algae) can be concentrated at prescribed vertical distance in the setup. The corresponding u_{rms} values ranged from 0.6 mm/s ($f = 1$ Hz) to 10.3 mm/s ($f = 6$ Hz). Normalized turbulence intensities, u_{rms}/f S and w_{rms}/f S, both decay with vertical distance from the grid. A power-law fit depicted the decay with exponents, -1.5 and -1.6, for u_{rms}/f S versus $z/\sqrt{\mathrm{SM}}$ and w_{rms}/f S versus $z/\sqrt{\mathrm{SM}}$, respectively.

Table 2 Fluid-flow conditions in the oscillating grid setup measured with PIV technique

Grid frequency	Vertical distance[a]	Energy dissipation rate[b]	Horizontal −root-mean −square velocity[b]	Vertical root-mean −square velocity[b]	$\frac{w_{rms}}{u_{rms}}$	Integral length scale[b]	Kolmogorov length scale[b]	Reynolds number
f(Hz)	z (mm)	ε_D(m^2/s^3) $\times 10^{-6}$	u_{rms}(mm/s)	w_{rms}(mm/s)	(−−)	l_o(mm)	η_k(mm)	Re_{l_o}(−−)
1	154	15.1	2.6	2.7	1.04	11.6	0.5	30
	222	4.1	1.2	1.3	1.08	13.3	0.7	16
	290	1.3	0.6	0.6	1.00	15.3	0.9	9
2	154	51.6	3.9	4.2	1.08	13.2	0.4	52
	222	8.3	2.1	2.3	1.10	14.5	0.6	30
	290	5.7	1.2	1.3	1.08	16.4	0.7	20
4	154	208.5	8.5	8.5	1.00	15.5	0.3	132
	222	52.0	5.2	4.4	0.85	17.8	0.4	43
	290	22.3	3.3	3.1	0.94	19.3	0.5	64
6	154	358.1	10.3	10.9	1.06	16.4	0.2	167
	222	93.5	7.5	6.1	0.81	18.5	0.3	139
	290	52.7	5.2	5.5	1.06	20.5	0.4	106

[a] Vertical distance from the grid mid-plane to the mid-plane of sampling locations a-b-c; d-e-f; and g-h-i (Fig. 1)

[b] Averaged at the same vertical distance (z) over the horizontal plane

Water kinematic viscosity, ν (at 20° C) = 10^{-6} m^2/s

6.2 Energy dissipation rate

The estimates of direct rate of energy dissipation (ε_D) obtained from the processed PIV data and calculated using Eq. 2 are reported in Table 2. The time-averaged energy dissipation rates were averaged over the LDV control volume and consequently were averaged over the three vertical distances ($z = 154, 222$, and 290 mm) in the setup (Table 2). The detailed comparison of ε_D at specific f and different distances from the oscillating grid confirmed a power scaling law$\varepsilon \sim z^{-4}$ [11]. The energy dissipation rates ranged from 1.2×10^{-9}($z = 420$ mm, $f = 1$ Hz; estimated by extrapolating the calculated ε_D at $z = 154, 222, 290$ mm) to 3.6^{-4}m^2/s^3 ($z = 154$ mm, $f = 6$ Hz). These values are within the range reported in natural and engineered aquatic ecosystems systems and are in agreement with the results reported in similar experimental setups [3,5,18].

6.3 Fluid-flow characteristic scales

The estimated energy dissipation rates at proposed sampling locations in the reactor were used to estimate the Kolmogorov micro scales (Table 2). The spatially averaged Kolmogorov scales ranged from 0.2 to 0.9 mm. Since velocity gradients with the PIV were resolved at a spatial scale of 0.54 mm, and the smallest spatially averaged Kolmogorov scale was around 0.2 mm, the velocity gradients were resolved at the order of $3\eta_K$ for the most energetic flow, $f = 6$ Hz, in the setup.

The integral length scale (l_o) provides a useful quantification of the extent of the region over which velocity fluctuations are appreciably correlated, i.e., the size of the large eddies. Integral length scales were estimated by numerically integrating the

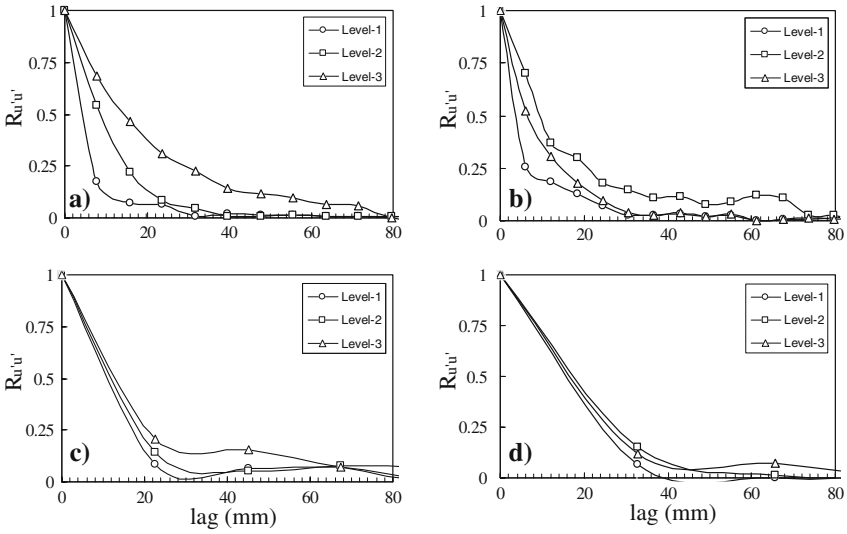

Fig. 3 Autocorrelation of horizontal velocity fluctuation ($R_{\acute{u}\acute{u}}$) for different oscillating frequencies at Levels (1–3) — location (**e**) and at the same vertical distance ($z = 222$ mm). **a** $R_{\acute{u}\acute{u}}$ at $f = 1$ Hz, **b** $f = 2$ Hz, **c** $f = 4$ Hz, and **d** $f = 6$ Hz

autocorrelation functions (Fig. 3). The integral time scale (τ) was estimated based on the autocorrelation function of the temporal LDV velocity data. The corresponding l_o was also calculated by multiplying the u_{rms} by τ and compared with the PIV results. The l_o calculated using PIV were on average 5% larger than the l_o calculated using the LDV. Both integral length scales exhibit an increase in value with z. LDV velocity data were obtained with 50 time faster frequency than the PIV data and therefore provided more reliable l_o. The averaged l_o estimated by LDV at each f were used as the scaling parameter in the normalized Euelrian frequency spectra. Although the Reynolds number $Re_{l_o} = \frac{u_{rms} l_o}{\nu}$ was not large ($9 < \frac{u_{rms} l_o}{\nu} < 167$), the energy spectral densities depicted the existence of the inertial subrange (Figs. 4, 5).

6.4 Eulerian frequency spectra

The LDV velocity data were used to obtain the Eulerian frequency spectrum (turbulent kinetic energy spectrum with time averaged velocity close to zero),$\phi(\omega)$, at all locations and for various f. The turbulent kinetic energy spectra and corresponding frequencies were normalized by the integral length scale (l_o) and the root-mean-square velocity components. The horizontal normalized energy spectra $\phi_u(\omega)$ and the vertical normalized power spectra $\phi_w(\omega)$ were plotted in Fig. 4 and 5. Inertial subrange depicted by the -5/3 slopes for both velocity components was evident. The inertial subrange was in the normalized frequency range about $40 > \frac{\omega l_o}{u_{\text{rms}}} > 3$. The normalized spectra obtained at various locations in the setup seem to collapse satisfactorily, indicating that the theoretical form using Eq. 1 to estimate the energy dissipation in the experimental setup was appropriate. The Kolmogorov eddies have an estimated frequency, ω_K, from 0.4 to 30 and thus the -5/3 slope behavior is expected in the normalized frequency range from $50 > \frac{\omega_K l_o}{u_{\text{rms}}} > 10$. De Silva and Fernando [22] reported the -5/3 behavior in the frequency range of $10 > \frac{\omega l_o}{u_{\text{rms}}} > 1.5$.

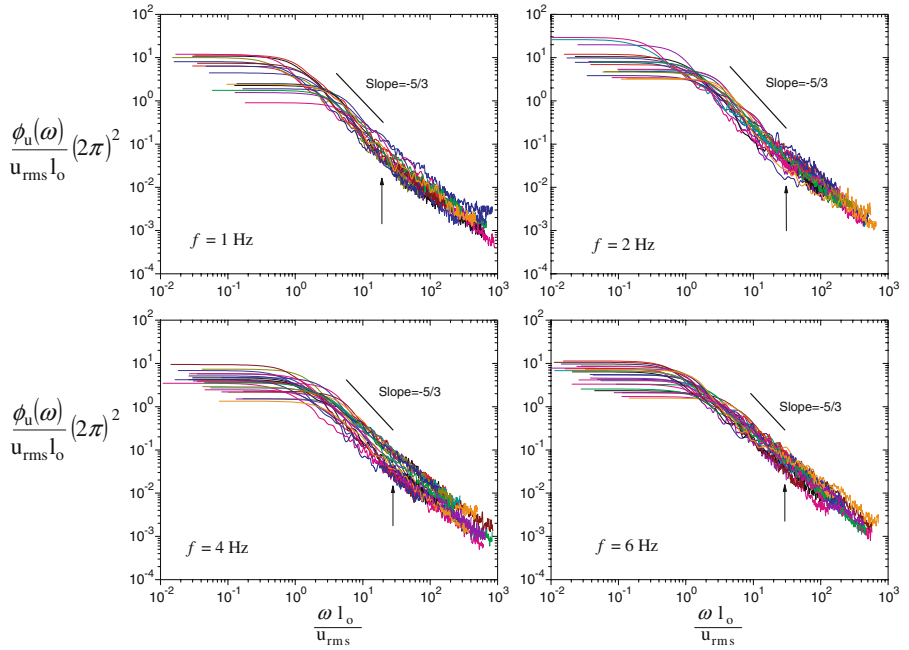

Fig. 4 Normalized energy spectra $\phi_u(\omega)$ for the horizontal velocity component (u) at 27 locations. ω is the angular frequency, $u_{\rm rms}$ is the root-mean-square velocity, and $l_{\rm o}$ is the length scale after which autocorrelation of the velocity component vanishes. *Arrows* indicate an upper limit in the inertial subrange

6.5 Constant (α) in the Eulerian spectrum

The universal constants α_u and α_w for the horizontal and vertical velocity components were estimated for $f = 1, 2, 4$ and 6 Hz at 27 measurement locations and generated data sets of about 80 α values. The $\varepsilon_{\rm D}$ obtained from PIV measurements, time-averaged and spatially averaged over the LDV sampling control volume, were used to normalize energy spectra obtained from the LDV data and consequently to provide estimates of $\alpha = \dfrac{\frac{\phi(\omega)}{u_{\rm rms}^4/\varepsilon_{\rm D}}}{\left(\frac{\omega\, u_{\rm rms}^2}{\varepsilon_D}\right)^{-5/3}}$ in accordance with Eq. 1 (Figs. 6 and 7) [7,12]. Only plots that indicated the existence of a $-5/3$ slope in the inertial subrange were used for the estimation of α. The $\alpha_{\rm u}$ values ranged from 0.4 to 2.1 and the α_w values ranged from 0.5 to 3.0. These estimates were in agreement with the values reported by previous researchers. Kit et al. [7] estimated $\alpha_u = 0.9$ and $\alpha_w = 0.7$, Bache and Rasool [11]]proposed a range $\alpha = 1.2 \pm 0.3$ (SD), Elsner and Elsner [12] reported $\alpha = 1.7$, Doron et al. [15] suggested $\alpha = 1.6$, and Hondzo and Lyn [1] used $\alpha_u = 0.8$. The variation among the values suggested by different investigations implied a continuing debate on the estimates of α value and its universality feature. The solid line of Figs. 6 and 7 depicts a $-5/3$ slope for the dimensionless frequency range $50 > \frac{u_{\rm rms}^2 \omega}{\varepsilon_D} > 3$ which confirmed our previous finding in analyzing the Eulerian frequency spectra.

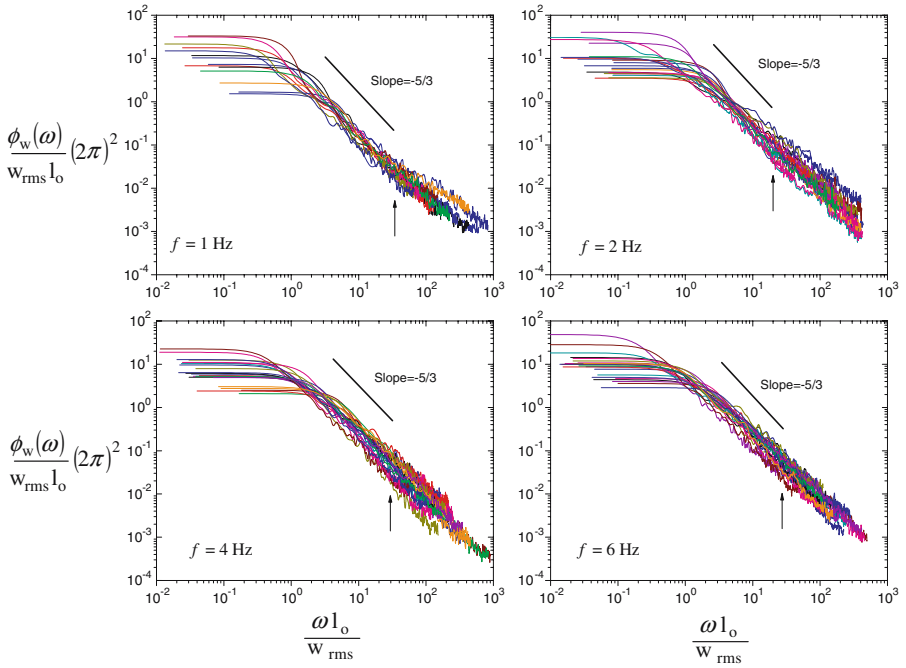

Fig. 5 Normalized energy spectra $\phi_w(\omega)$ for the vertical velocity component (w) at 27 locations. w_{rms} is the root-mean-square velocity

The statistical analyses of α data revealed that α can be described, satisfying the chi-square (χ^2) test at the significance level of 95.5%, by a lognormal probability distribution (Fig. 8). First statistical moments for the lognormal distribution for all f were $\bar{\alpha}_{\mathrm{u}} = 1.16$ and $\bar{\alpha}_w = 1.35$ with second statistical moments of 0.62 and 0.57, respectively. In order for α to encompass a 95.5% below the lognormal probability distribution $\alpha_u$should be in the range $\bar{\alpha}_u \left(\sigma_{\alpha_u}\right)^2 \leq \alpha_u \leq \frac{\bar{\alpha}_u}{\left(\sigma_{\alpha_u}\right)^2}$, i.e., $2.91 \geq \alpha_u \geq 0.43$and α_w should be in the range $4.44 \geq \alpha_{\mathrm{w}} \geq 0.42$. Statistical moments for different frequencies of the oscillating grid are provided in Table 3. For each oscillating frequency, the estimates of α followed the lognormal probability distribution.

7 Conclusions

Turbulent fluid-flow conditions were quantified in an oscillating grid setup using LDV and PIV measuring techniques. The rate of dissipation of turbulent kinetic energy in the setup ranged from 10^{-9} to $10^{-4}\,\mathrm{m^2/s^3}$ and was similar to the levels of energy dissipation commonly reported in engineered and natural aquatic ecosystems. Time-averaged velocities were close to zero with turbulent fluctuations ratios on the order of (1) indicating nearly isotropic fluid-flow conditions in the setup. The velocity spectra, obtained by stationary LDV measurements for the vertical and horizontal velocity components across the setup, indicated the existence of an inertial subrange with the "$\omega^{-5/3}$" power law scaling. The estimated Eulerian frequency spectrum followed the

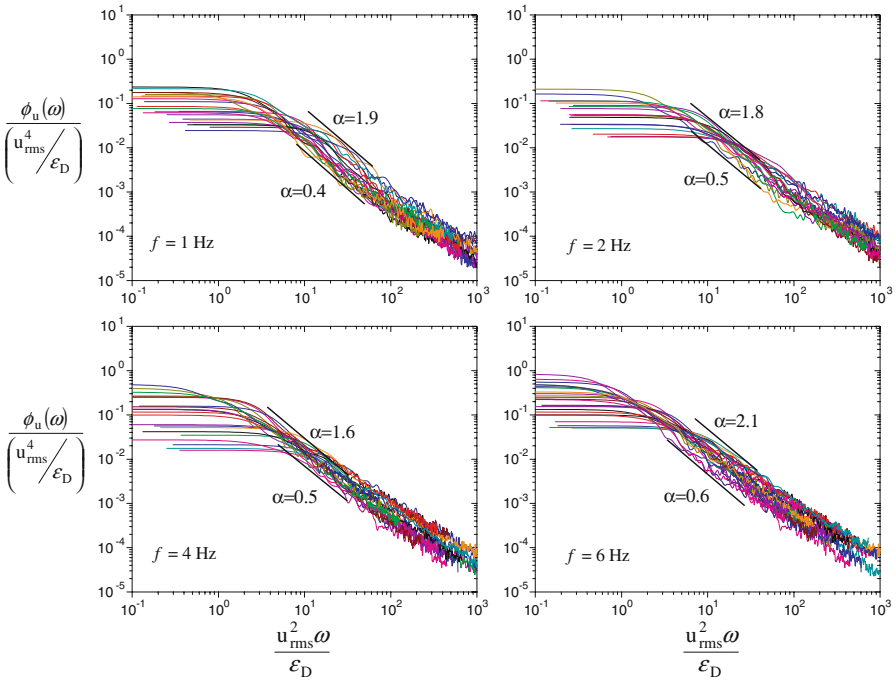

Fig. 6 Normalized energy spectra $\phi_u(\omega)$for the horizontal velocity (u) at 1, 2, 4, and 6 Hz oscillating grid frequency. Measurements were conducted at 27 locations in the experimental setup using the LDV. The energy spectra were normalized by the corresponding dissipation rate (ε_D) measured at the same location using the PIV

Table 3 Estimated first ($\bar{\alpha}$) and second (σ_α) statistical moments of constant with the interval of 95.5% following the lognormal probability distribution

Grid frequency f(Hz)	The first statistical moment of the horizontal constant $(\bar{\alpha})_u$ (−−)	The second statistical moment of the horizontal constant σ_{α_u}(−−)	Log-normally distributed $(\bar{\alpha})_u$with interval of 95.5%[a] (−−)	The first statistical moment of the vertical constant $(\bar{\alpha})_w$ (−−)	The second statistical moment of the vertical constant σ_{α_w}(−−)	Log-normally distributed $(\bar{\alpha})_w$ with interval of 95.5%[a] (−−)
1	0.82	0.29	0.1–9.7	1.13	0.55	0.3–3.7
2	1.61	0.65	0.7–3.8	1.76	0.87	1.3–2.3
4	1.03	0.48	0.2–4.5	1.35	0.69	0.6–2.8
6	1.92	0.68	0.9–4.2	2.05	0.86	1.5–2.8

[a] $\left(\frac{\bar{\alpha}}{\sigma^2}\right) > \alpha > \bar{\alpha}\sigma^2$ (95.5%)

theoretical functional relation proposed by Tennekes [6] and confirmed the applicability of the inertial dissipation method for estimating the rate of dissipation of turbulent kinetic energy. PIV was used for a direct estimation of dissipation by evaluating spatially distributed velocity gradients. The direct dissipation estimate in conjunction with the estimated Eulerian frequency spectrum provided evaluation of the "universal" constant α in the functional relationship proposed by Tennekes. The value of α was

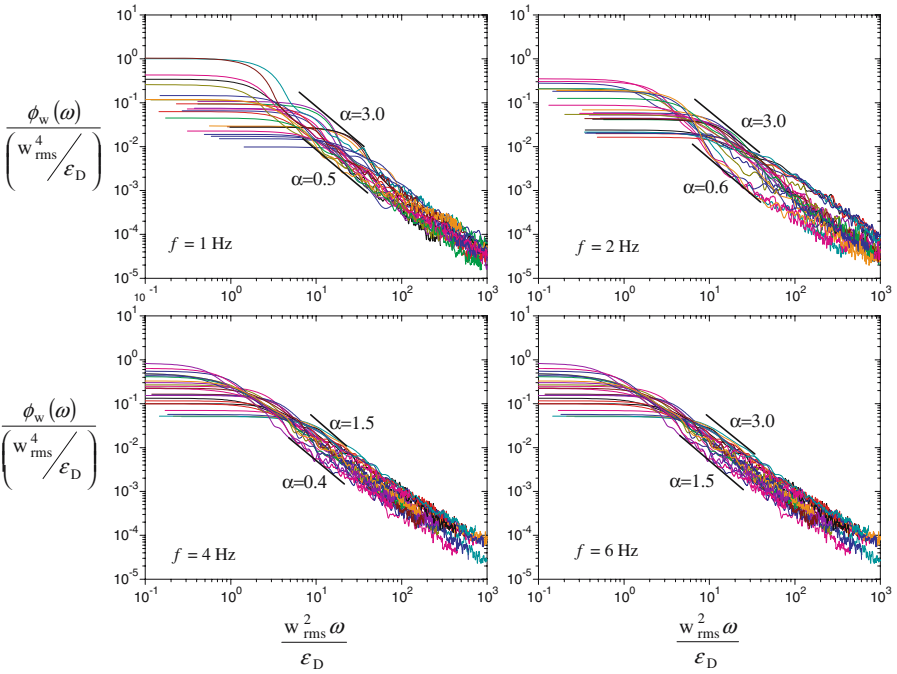

Fig. 7 Normalized energy spectra $\phi_w(\omega)$ in the x-direction for the vertical velocity (w) at 1, 2, 4, and 6 Hz oscillating grid frequency

Fig. 8 **a** The probability distribution of α_u at all measurement locations for $f = 1, 2, 4$, and 6 Hz, and **b** the probability distribution of α_w. Superimposed on the plots are the lognormal probability distribution curves. n is the number of data points

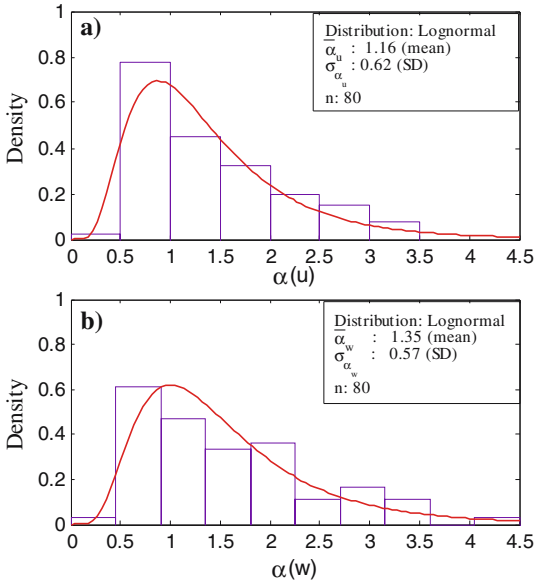

not constant. The estimates followed a lognormal probability distribution for vertical and horizontal velocity components. In order to encompass a 0.955 probability range under the lognormal distribution $\left(\frac{\bar{\alpha}}{\sigma^2} > \alpha > \bar{\alpha}\sigma^2\right)$ the universal constant was in the range $2.91 \geq \alpha_u \geq 0.43$ and $4.44 \geq \alpha_w \geq 0.42$ for horizontal and vertical velocity components, respectively.

List of Symbols

ADV	acoustic-Doppler velocimeter
d_m	control volume diameter (LDV)
f	oscillating grid frequency
k	wave number
l	wavelength corresponding to k
LDV	laser-Doppler velocimeter
l_m	control volume length (LDV)
l_o	integral length scale
M	spacing between rods (mesh size)
PIV	particle image velocimetry
Re_{l_o}	Reynolds number
$R_{\acute{u}\acute{u}}$	autocorrelation function
S	stroke length
SD	standard deviation
u	horizontal velocity component in the x-direction
u'	fluctuating horizontal velocity u
$\bar{u}$	time average velocity u
$\bar{u}_\mathrm{LDV}$	time average velocity u using LDV
$\bar{u}_\mathrm{PIV}$	time average velocity u using PIV
u_rms	horizontal root-mean-square velocity
u_rmsLDV	horizontal root-mean-square velocity using LDV
u_rmsPIV	horizontal root-mean-square velocity using PIV
w	vertical velocity component in the z-direction
w'	fluctuating vertical velocity w
$\bar{w}$	time average velocity w
$\bar{w}_\mathrm{LDV}$	time average velocity w using LDV
$\bar{w}_\mathrm{PIV}$	time average velocity w using PIV
w_rms	vertical root-mean-square velocity
w_rmsLDV	vertical root-mean-square velocity using LDV
w_rmsPIV	vertical root-mean-square velocity using PIV
x	Cartesian coordinate in the horizontal direction
z	Cartesian coordinate in the vertical direction
α	universal constant
α_u	universal constant for u velocity component
$\bar{\alpha}_\mathrm{u}$	first statistical moment of α_u
α_w	universal constant for w velocity component
$\bar{\alpha}_\mathrm{w}$	first statistical moment of α_w
ε	energy dissipation rate

ε_D	energy dissipation rate direct estimate
η_K	Kolmogorov scale
ν	kinematic viscosity
σ	standard deviation
σ_{α_u}	the second statistical moment of α_u
σ_{α_w}	the second statistical moment of α_w
τ	integral time scale
$\phi(\omega)$	the kinetic energy per unit frequency
χ^2	chi-square
ω	frequency
ω_K	Kolmogorov frequency

Acknowledgements This study was funded by US Army Corps of Engineers—Chicago District through US Army of Corps of Engineers, Waterways Experiment Station, Vicksburg, Mississippi. Contract numbers at the University of Minnesota were DACW42-00-p-0123 "Analysis of Oxygen Demand in Reservoirs with Bubble Diffusers," and DACW42-01-C-0014 "Oxygen Demand Caused by Sediment and Biochemical Degradation in Combined Sewer Overflow." Partial support for this work is also provided by the National Center for Earth-surface Dynamics (NCED), a Science and Technology Center funded by the Office of Integrative Activities of the National Science Foundation (under agreement Number EAR- 0120914). We thank Dr. M. Wosnik and Dr. M. Carper, St. Anthony Falls Laboratory, University of Minnesota, for their valuable assistance with the PIV measurements.

References

1. Hondzo M, Lyn D (1999) Quantified small-scale turbulence inhibits the growth of a green alga. *Freshw Biol* 41:51–61
2. Warnaars TA, Hondzo M, Carper M (2006) Small-scale fluid motion mediates growth and nutrient uptake of *Selenastrum capricornutum*. *Freshw Biol* 51:999–1015
3. Al-Homoud A, Hondzo M, LaPara T (2007) The impact of fluid dynamics on bacterial physiology: implications for the measurements of biochemical oxygen demand. *J Environ Eng* 1133(2):226–236
4. American Public Health Administration (APHA) (1998) Standard methods for the examination of water and wastewater, 19th edn. Washington, DC
5. Bregstedt M, Hondzo M, Cotner JB (2004) Effect of small scale fluid motion on bacterial growth and respiration. *Freshw Biol* 49:28–40
6. Tennekes H (1975) Eulerian and Lagrangian time microscales in isotropic turbulence. *J Fluid Mech* 67:561–567
7. Kit E, Fernando HJS, Brown JA (1995) Experimental examination of Eulerian frequency spectra in zero-mean-shear turbulence. *Phys Fluids* 7:1168–1170
8. Gross TF, Nowell ARM (1985) Spectral scaling in a tidal boundary layer. *J Phys Oceanogr* 15:496–508.
9. Dewey RK, Crawford WR (1988) Bottom stress estimates from vertical dissipation rate profile on the continental shelf. *J Phys Oceanogr* 18(8):1167–1177
10. Mansour NN, Wray AA (1994) Decay of isotropic turbulence at low Reynold number. *Phys Fluids* 6:808–814
11. Bache DH, Rasool E (1996) Measurement of the rate of dissipation around an oscillating grid by an energy balance approach. *Chemical Eng Journal*. 63:105–115
12. Elsner JW, Elsner W (1996) Review article on the measurement of turbulence and dissipation. *Meas Sci Technol* 7:1334–2348
13. Lien R, D'Asaro EA, Dairiki GT (1998) Lagrangian frequency spectra of vertical velocity in high-Reynolds-number ocean turbulence. *J Fluid Mech* 362:177–198
14. Bertuccioli L, Roth GI, Katz J, Osborn TR (1999) A submersible particle image velocimetry system for turbulence measurements in the bottom boundary layer. *J Atmos Ocean Tech* 16:1635–1646
15. Doron P, Bertuccioli L, Katz J (2001) Turbulence characteristics and dissipation estimates in coastal ocean bottom boundary layer from PIV data. *J Phys Oceanogr* 31:2108–1134

16. Gotoh T, Fukayama D, Nakano T (2002) Velocity field statistics in homogenous steady turbulence obtained using a high-resolution direct numerical simulation. *Phys Fluids* 14:1065–1081
17. Lorke A, Wüest A (2005) Application of coherent ADCP for turbulent measurements in the bottom boundary layer. *J Atmos Ocean Tech* 22:1821–1828
18. O'Brien KR, Meyer DL, Waite AM, Ivey GN, Hamilton DP (2004) Disaggregation of *Microcystic aeruginosa* colonies under turbulent mixing: laboratory experiment in a grid-stirred tank. *Hydrobiologia* 519:143–152
19. Soga CLM, Rehmann CR (2004) Dissipation of turbulent kinetic energy near a bubble plume. *J Hydraul Eng* 130:441–449
20. Pope SB (2000) Turbulent flows. Cambridge University Press, New York
21. Westerweeler J (1997) Fundamental of digital particle image velocimetry. *Meas Sci Technol* 8:1379–1392
22. De Silva IPD, Fernando HJS (1994) Oscillating grid as a source of nearly isotropic turbulence. *Phys Fluids* 6:2455–2466
23. Webster DR, Brathwaite A, Yen J (2004) A novel laboratory apparatus for simulating isotropic oceanic turbulence at low Reynolds number. *Limnology and Oceanogr Methods* 2:1–22